

- ter, *Z. Phys. B* **72**, 497 (1988); J. K. Gimzewski, J. K. Sass, R. R. Schlittler, J. Schott, *Europhys. Lett.* **8**, 435 (1989).
5. R. Berndt, J. K. Gimzewski, P. Johansson, *Phys. Rev. Lett.* **67**, 3796 (1991).
 6. R. Gaisch *et al.*, *Ultramicroscopy* **42**, 1621 (1992).
 7. T. Hashizume *et al.*, *Jpn. J. Appl. Phys.* **31**, L880 (1992); Y. Z. Li *et al.*, *Science* **252**, 547 (1991); H. P. Lang *et al.*, *Europhys. Lett.* **18**, 29 (1992); J. L. Wragg *et al.*, *Nature* **348**, 623 (1990); R. J. Wilson *et al.*, *ibid.*, p. 621; E. I. Altman and R. J. Colton, *Surf. Sci.* **279**, 49 (1992); T. Chen *et al.*, *Phys. Rev. B* **45**, 14411 (1992); R. Gaisch *et al.*, *Appl. Phys. A* **57**, 207 (1993).
 8. B. N. J. Persson and A. Baratoff, *Phys. Rev. Lett.* **68**, 3224 (1992).
 9. A. Otto, I. Mrozek, H. Grabhorn, W. Akemann, *J. Phys. Condens. Matter* **4**, 1143 (1992).
 10. R. Berndt and J. K. Gimzewski, *Phys. Rev. B* **48**, 4746 (1993).
 11. R. Berndt, thesis, University of Basel, Basel, Switzerland (1992).
 12. E. V. Albano, S. Daiser, R. Miranda, K. Wandelt, *Surf. Sci.* **150**, 386 (1985).
 13. C. Reber *et al.*, *J. Phys. Chem.* **95**, 2127 (1991); M. Matus, H. Kuzmany, E. Sohmen, *Phys. Rev. Lett.* **68**, 2822 (1992).
 14. A. T. Werner *et al.*, *Europhys. Conf. Abstr.* **17A**, 1854 (1993).
 15. A. Lucas *et al.*, *Phys. Rev. B* **45**, 13694 (1992); M. T. Michalewicz and M. P. Das, *Solid State Commun.* **84**, 1121 (1992).
 16. We thank R. L. Whetten for providing the fullerene molecules, W. Andreoni and M. Parrinello for useful discussions, and Ch. Gerber and H. Rohrer for their support. Supported in part by the Swiss National Science Foundation programs NFP24 and NFP24+.

16 August 1993; accepted 26 October 1993

X-ray Linear Dichroism Microscopy

H. Ade* and B. Hsiao

Chemical-specific x-ray linear dichroism was observed in an x-ray microscope as evidenced by changes in relative contrast upon azimuthal rotation of the sample. As a demonstration, thin sections of a partially ordered polymer fiber were examined with a transmission x-ray microscope near the carbon K-shell absorption edge to provide chemical-specific imaging at 50-nanometer spatial resolution. The observed dichroism and change in contrast upon rotation arise from the polarization dependence of the near-edge x-ray absorption cross section and can be used to image the orientation of specific chemical bonds.

The structural, morphological, and chemical characterization of multiphase polymers, liquid crystalline polymers, fibers, and composites is critical to our understanding of the mechanical and chemical properties of these materials. A variety of characterization techniques have been used, ranging from electron microscopy to neutron scattering (1, 2). None of these techniques can, however, provide information about the orientation of specific chemical bonds in nonisotropic samples at suboptical spatial resolution. We present a technique, x-ray linear dichroism microscopy, that can acquire such information at 50-nm spatial resolution. Another kind of dichroism microscopy, x-ray circular dichroism microscopy, has recently been developed by Stöhr *et al.* (3). It provides element-specific magnetization contrast between magnetic domains at a spatial resolution of about 1 μm and addresses a set of applications different from those addressed by the technique presented here.

To demonstrate x-ray linear dichroism microscopy, we used the scanning transmission x-ray microscope (STXM) at the National Synchrotron Light Source (NSLS). Soft x-rays generated by the X1 undulator at NSLS were used, and the microscope's imaging characteristics and performance have been de-

scribed previously (4). We added an azimuthally rotatable sample stage to the microscope (5). We also made use of the linear polarization of the undulator output, which is a characteristic of synchrotron radiation so far unexploited in x-ray microscopy. We imaged thin sections of poly(*p*-phenylene terephthalamide) (PPTA) fibers (Kevlar) with a spatial resolution of 50 nm at photon energies that are sensitive to the carbonyl and the aromatic groups of the fiber polymer. Three types of Kevlar fibers were chosen: Kevlar 29, 49, and 149, which differ from each other in the degree of crystallinity (Kevlar 149 is the most and Kevlar 29 is the least crystalline) and the crystalline orientation along the fiber axis (6).

We observed x-ray linear dichroism at high spatial resolution in all samples. This is to be expected for a partially oriented and ordered sample such as Kevlar because the near edge x-ray absorption fine structure (NEXAFS) is not only chemically sensitive, but the near edge cross sections strongly depend on the geometric orientation of the chemical bond relative to the electric field vector (7). We observed butterfly-like patterns for all of these fibers, consistent with radially symmetric models of the fiber structure. In addition, some thin films of similar Kevlar fibers, prepared separately, exhibited a one-dimensional anisotropy, presumably introduced by the stress during sectioning. These films showed pronounced contrast

changes upon rotation and features predominantly oriented perpendicular to the cutting direction.

A small-area spectrum of a Kevlar 49 thin film (0.1 μm thick) cut at 45° relative to the fiber axis as acquired with the STXM is shown in Fig. 1. The most prominent peaks are associated with aromatic (285.5 and 286.3 eV) and carbonyl (288.3 eV) groups. The photon energy can be selectively tuned to these characteristic energies to achieve chemical sensitivity during imaging (8); owing to the polarization dependence of NEXAFS, the strong peak at 285.5 eV, for example, would actually disappear if all the aromatic groups were lying in a single plane and the electric field vector of a 100% polarized x-ray beam was also lying in the same plane. The physics of this process is well understood. The intensity observed is proportional to $\cos^2\theta$, where θ is the angle between the electric field vector and the direction of the orbital excited during absorption, which for a π orbital is perpendicular to the aromatic plane (7).

The radially symmetric structural model of Kevlar fibers predicts the observation of a butterfly-like pattern in an x-ray linear dichroism image of thin films of the fiber cut at 45° with respect to the fiber axis (9). The planes of the two different aromatic groups of the fiber are not the same. They are estimated to be at an angle of 68° with respect to each other (6), with the average aromatic ring plane pointing essentially radially outward. Thus, the maximum observable contrast in an image acquired at 285.5 eV is reduced significantly compared with that achievable in a sample having a single aromatic plane. This results in about 15% contrast, which is further reduced by orientational disorder and the

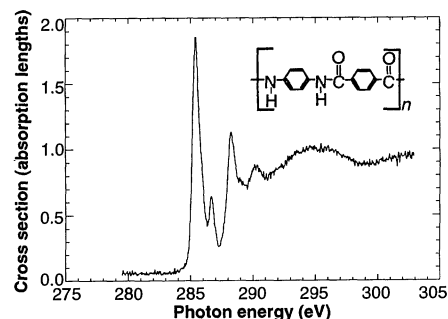


Fig. 1. The NEXAFS spectrum of 0.1 μm^2 of a 0.1- μm -thick section of Kevlar 49 fiber (inset structure) cut at 45° as acquired with the STXM. The prominent spectral features at 285.5, 286.7, and 288.3 eV are π^* resonances associated with unsaturated bonding in the aromatic and carbonyl groups. The energies are characteristic, providing the means for bond-selective imaging, whereas the intensity depends on polarization and the geometrical orientation of the bonds. The broader feature at 295 eV is a σ^* resonance of the C-C bonds. Total acquisition time was 40 s (13).

H. Ade, Department of Physics, North Carolina State University, Raleigh, NC 27695-8202.
B. Hsiao, Experimental Station, DuPont, Wilmington, DE 19880-0302.

*To whom correspondence should be addressed.

pleated structure observed and proposed by Dobbs *et al.* (10). Despite this reduction in contrast to the several-percent level, we successfully observed butterfly patterns. The patterns, indicating an overall radial orientation of the aromatic groups in the fiber, are readily observable if we reverse the contrast in images with the electric vector rotated by about 90° relative to each other (Fig. 2). The blue regions of the image correspond to high absorption, consistent with the structural model and the average aromatic plane pointing out-

wards. The roughly parallel features overlying the butterfly pattern are thickness variations caused by the sectioning and are perpendicular to the cutting direction.

We also acquired sets of images of several Kevlar 149 fibers from a different batch of sections at 285.5 and 288.3 eV, rotated in increments of about $\pi/8$ radians over a total of π radians (Fig. 3). Again, relative contrast changes reflecting x-ray linear dichroism are evident in most areas of the fibers for the two orientations shown. In contrast to Fig. 2, the

features in these images exhibit high contrast and a pronounced preferential orientation. We believe the observed structures to be anisotropies induced by the stress present during sectioning (11). Owing to their high contrast, they overshadow the underlying low-contrast butterfly pattern that is just barely noticeable in some of the fibers. Although the overall orientation of the bonds as a function of location is complex in these altered samples, qualitative analysis of the data does show, for example, that the projected carbonyl bonds are predominantly oriented in the left-right direction in areas that have the highest relative contrast change and are bright in Fig. 3A and dark in Fig. 3B. Because the image formation of our technique uses absorption contrast, just as regular imaging with the STXM, the spatial resolution achievable in images containing orientational information remains unchanged by our extension of the STXM capabilities. The present Rayleigh resolution limit is about 50 nm, which corresponds to a visibility limit of 30 nm (4, 12).

With regard to the spatial resolution, one of the most fundamental parameters of a microscope, the STXM holds an intermediate position. Its resolution exceeds visible and infrared microscopes by about an order of magnitude but falls short of the very high resolution offered by electron and scanning probe microscopes (12). However, x-ray microscopy has unique contrast mechanisms, and the general advantages of NEXAFS imaging, such as chemical sensitivity and low beam damage, have recently been demonstrated and discussed by Ade *et al.* (8). In particular, the directional and chemical sensitivity can to some extent only be provided by infrared dichroism, albeit at a much reduced spatial resolution of a few micrometers. Dark-field imaging in electron microscopes requires crystallographic order and lacks chemical sensitivity. Electron energy loss spectroscopy (EELS) imaging has chemical, but in general not orientational, sensitivity and imparts a heavy radiation dose to the sample (1, 8). Visible light microscopy with crossed polars has been used extensively as a characterization tool to assess directional order through birefringence, but it generally lacks chemical sensitivity and has reduced spatial resolution when compared with x-ray microscopy (1). In addition, the detection of the Auger, secondary electron, and fluorescent yield could be incorporated into an x-ray microscope without loss of chemical and orientational sensitivity. The NEXAFS imaging technique would be capable of adjusting the surface sensitivity from 0.5 nm (Auger yield) to 0.2 μm (fluorescent yield) for carbon NEXAFS imaging (7). This would prevent the need for the preparation of thin samples, as is necessary for many types of microscopes, and would provide a means for the investigation of the chemical and orientational characteristics

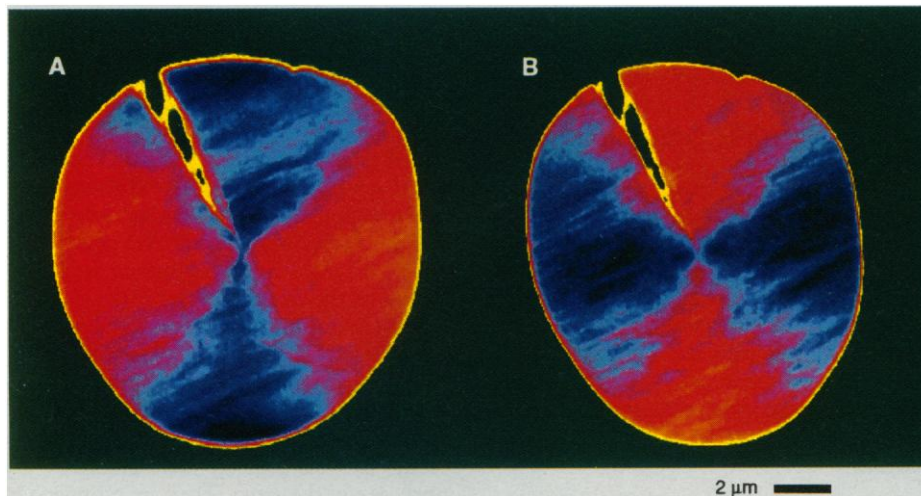


Fig. 2. Images of an embedded and sectioned (0.2 μm thick) Kevlar 149 fiber acquired at a photon energy of 285.5 eV. The electric field vector is in the left-right (A) and up-down (B) direction. Butterfly-like patterns are observable in both images, and the pattern rotates with the rotation of the electric field vector. This is consistent with the expected x-ray dichroism of a radially symmetric structure. The radial feature in the upper left part is a crack in the fiber. The sample's shape appears to differ in the two images because of different distortions. The transition from black to blue, light blue, pink, red, orange, and yellow is from high to low absorption.

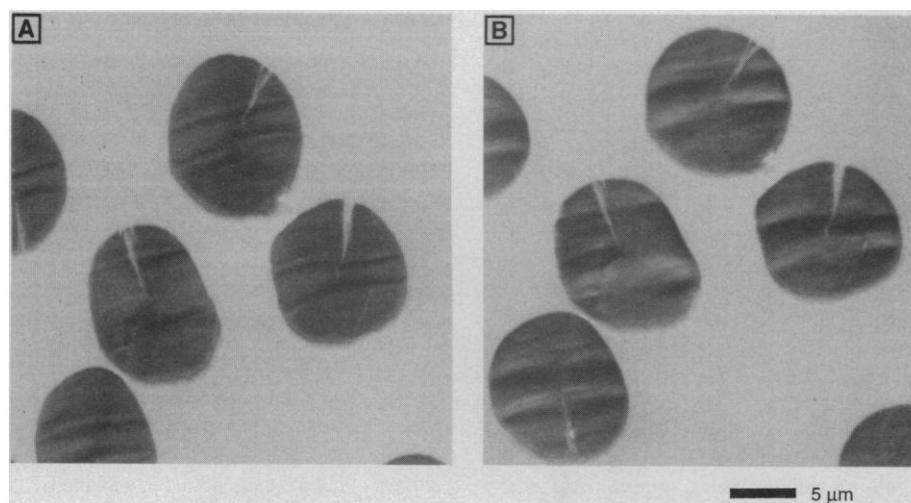


Fig. 3. Images of several embedded and sectioned (0.1 μm thick) Kevlar 149 fibers acquired at the carbonyl absorption peak at 288.3 eV, with the electric field vector in the (A) left-right and (B) up-down direction. The cutting direction is close to the up-down direction and hence approximately parallel (B) and perpendicular (A) to the field vector. Features with the largest relative contrast change, which appear dark in (A) and bright in (B), have the carbonyl group predominantly aligned in the up-down direction, whereas features bright in (A) and dark in (B) have the carbonyl group predominantly aligned in the left-right direction. Note that all fibers have cracks. Owing to different magnifications in the two images, the sample area imaged is slightly different in these micrographs (400 pixels by 400 pixels, 5-ms dwell).

of thick samples, such as fracture surfaces, directly.

We anticipate that applications of this technique will comprise the characterization of phase-separated and -oriented polymeric alloys and their interfaces, composites, diamond-like carbon films, other carbon-containing advanced materials, as well as coal and coke. Absorption edges of elements other than carbon, particularly those of nitrogen and oxygen, could also be explored.

REFERENCES AND NOTES

1. L. C. Sawyer and D. T. Grubb, *Polymer Microscopy* (Chapman and Hill, New York, 1987).
2. R. S. Stein and C. C. Han, *Phys. Today* 1, 74 (1985).
3. J. Stöhr *et al.*, *Science* 259, 658 (1993).
4. C. Jacobsen *et al.*, *Opt. Commun.* 86, 351 (1991); X. Zhang, C. Jacobsen, S. Williams, *Proc. SPIE* 1741, 251 (1993).

5. The rotation is in the plane of the sample surface, with the sample mounted perpendicular to the propagation direction of the x-ray beam.
6. H. H. Yang, *Aromatic High Strength Fibers* (Wiley-Interscience, New York, 1989).
7. J. Stöhr, *NEXAFS Spectroscopy* (Springer, Berlin, 1992); D. A. Outka *et al.*, *Phys. Rev. Lett.* 59, 1321 (1987); C. Tourillon *et al.*, *Surf. Sci.* 201, 171 (1988).
8. H. Ade *et al.*, *Science* 258, 972 (1992).
9. Sectioning perpendicular, rather than at 45°, to the fiber axis would have been preferable because this would have increased the observable contrast. However, owing to the mechanical properties of the fibers, it is impossible to do so.
10. M. D. Dobb, D. J. Johnson, B. P. Saville, *J. Polym. Sci. Polym. Phys. Ed.* 15, 2201 (1977).
11. The differences between Figs. 2 and 3 are not attributable to the change in photon energy, and therefore, mapping of a different functional group, but rather reflect a structural difference. We acquired images at photon energies of 285.5 eV that appear similar to the ones in Fig. 3.
12. C. Jacobsen, J. Kirz, S. Williams, *Ultramicroscopy* 47, 55 (1992).
13. We chose dwell times of about 80 ms per data

point to average over 12-Hz noise in the incident x-ray beam. Overflow of the scalars at this dwell time required aperturing down of the x-ray beam. We have since upgraded the electronics, and a 40-s spectrum with similar energy resolution would have almost 10 times the number of counts and therefore improved statistics and reduced noise.

14. We are grateful to the many people who have made this work possible. In particular, we thank J. Kirz and C. Jacobsen and their co-workers at the State University of New York (SUNY), Stony Brook, and the NLSL, who built and maintain the STXM, Sue Wirick for building a rotating sample mount, S. Subramoney for providing the samples, and A. Smith for helping with the data acquisition. J. Kirz also read the first draft of the manuscript and made helpful suggestions. Part of this work was performed while H.A. was at SUNY, Stony Brook, and was partly supported by the National Science Foundation (DIR 9005893). The work was performed at NLSL, which is supported by the Department of Energy, Office of Basic Energy Sciences.

20 July 1993; accepted 6 October 1993

Refuge Theory and Biological Control

Bradford A. Hawkins,* Matthew B. Thomas, Michael E. Hochberg

An important question in ecology is the extent to which populations and communities are governed by general rules. Recent developments in population dynamics theory have shown that hosts' refuges from their insect parasitoids predict parasitoid community richness patterns. Here, the refuge theory is extended to biological control, in which parasitoids are imported for the control of insect pests. Theory predicts, and data confirm, that the success of biological control is inversely related to the proportion of insects protected from parasitoid attack. Refuges therefore provide a general mechanism for interpreting ecological patterns at both the community level (their species diversity) and population level (their dynamics).

The practice of introducing parasitoids, those insects that parasitize and kill their arthropod hosts, for the biological control of insect pests has contributed much to ecological theory. Unfortunately, the converse is not true (1), because analytical parasitoid-host models that have been applied to biological control (2) have not identified simply measured, unambiguous parameters that actually improve the chances of successful pest control. Consequently, the practice of biological control through the introduction of natural enemies remains largely empirical and based on trial and error, in spite of the need to improve its scientific basis (3, 4).

We propose that theory recently developed to account for variability in the species richness of parasitoid communities of-

fers a simple methodology to evaluate the extent to which a parasitoid introduction will control a pest population. The model formalizing the theory (5, 6) identifies pro-

portional refuges from parasitism [defined as a fixed proportion of the host population immune to attack (7)] as a key constraint on the number of parasitoid species that can persist on a host (5). As a result of its population-dynamic structure, the model further quantifies the extent that parasitoids will depress host populations below the densities hosts would achieve in the absence of parasitoids (6).

It is this second property of the model that is relevant to biological control, the goal of which is to reduce and maintain pest populations below some critical density defined as their economic threshold. Basically, refuge theory predicts that hosts that occupy small refuges (that is, a low proportion of their population is in the refuges) will be highly exploitable by parasitoids, and as a result the host populations will be

B. A. Hawkins, Natural Environment Research Council Centre for Population Biology, Imperial College, Silwood Park, Ascot, Berks SL5 7PY, United Kingdom. M. B. Thomas, Leverhulme Unit for Population Biology and Biological Control, Imperial College, Silwood Park, Ascot, Berks SL5 7PY, United Kingdom. M. E. Hochberg, Ecole Normale Supérieure, CNRS-URA 258, Laboratoire d'Ecologie, 75230 Paris Cedex 05, France.

*To whom correspondence should be addressed.

Fig. 1. Relation between maximum percentage parasitism (in two cases including host mortality from host feeding by the parasitoid) and the outcome of parasitoid introductions for classical biological control. Multiple cases are denoted by larger circles. Blackened symbols represent failures and partial successes attributed to climatically related factors. The regression line illustrated is based on a logistic regression when partial successes have been excluded (logity = -2.880 + 0.057x, $\chi^2 = 28.48$, $n = 64$, $P < 0.0000001$). Regressions based on an economic evaluation of success (less than full control considered a failure) and a dynamic evaluation of success (full and partial successes taken as equal evidence of the ability of parasitoids to reduce pest densities) produced similar statistics (logity = -2.957 + 0.048x, $\chi^2 = 23.76$, $n = 74$, $P = 0.0000011$ and logity = -2.669 + 0.058x, $\chi^2 = 29.67$, $P < 0.0000001$, respectively).

